UDK 519.718:661.842:622.785

Structure and Magnetic Investigations of $Ca_{1-x}Y_xMnO_3$ (x=0, 0.1, 0.2, 0.3) and Mn^{4+}/Mn^{3+} Relation Aanalysis

J. Zagorac[1*], **S. Bošković**[1], **B. Matović**[1], **B. Babić-Stojić**[2]

[1] Vinča Institute of Nuclear Sciences, Laboratory of Material Science, P. O. Box 522, 11001 Belgrade, Serbia
[2] Vinča Institute of Nuclear Sciences, Laboratory of Radiation Chemistry and Physics, Belgrade, Serbia

Abstract:

   Structure and magnetic features of nanostructured materials with general formula $Ca_{1-x}Y_xMnO_3$ (x = 0; 0.1; 0.2; 0.3) were investigated. Goldschmidt tolerance factor, G_t and global instability index, GII were calculated for $Ca_{1-x}Y_xMnO_3$ (x = 0, 0.25, 0.5, 0.75, 1) using the software SPuDS (Structure Prediction Diagnostic Software). According to these two parameters possibility of forming perovskite structure type for $Ca_{1-x}Y_xMnO_3$ solid solution was analysed.

   Substitution of Y^{3+} for Ca^{2+} provokes reduction of equivalent amount Mn^{4+} into Mn^{3+}, the presence of which is a reason for many interesting magnetic, transport and structural features of doped $CaMnO_3$. Crystal structure refinement was carried out using Rietveld analysis. $Ca_{1-x}Y_xMnO_3$ (x = 0; 0.1; 0.2; 0.3) has an orthorombic, Pnma space group that, according to Glazer′s classification belongs to $a^-b^+a^-$ tilt system. Influence of Y amount on Mn–O bond angles and distances, tilting of MnO_6 octahedra around all three axes and octahedra deformation were analysed. Bond valence calculations (BVC) were performed to determine Mn valence state. Using EPR (electron paramagnetic resonance) magnetic measurements were performed and magnetic properties of solid solutions, orthorombicity degree of unit cell, as well as Mn^{4+}/Mn^{3+} cations ratio in position B were analysed. Microstructure size-strain analysis was performed and these results are in nanometric range which is confirmed by TEM images.

Keywords: _Nanostructured materials, Rietveld analysis, BVC calculations, Magnetic properties._

Introduction

   The doped manganites with general formula $A_{1-x}RE_xMnO_3$, where RE is a trivalent rare earth ion, have attracted great interest because many of these materials exhibit colossal magnetoresistance phenomena [1] and acceptable levels of electrical conductivity for cathode materials used for solid oxide fuel cells operation [2].

   $Ca_{1-x}Y_xMnO_3$ has a perovskite structure type that is very frequent in solid-state inorganic chemistry. The ideal perovskite structure for oxides has ABO_3 stoichiometry and is composed of a three-dimensional framework of corner-sharing BO_6 octahedra [3]. Athough the ideal perovskite structure is cubic, the small ionic radius of the Y (table 1) compared with the voids

_____

*) **Corresponding author:** dukicjelena@Yahoo.com

between the octahedra will result in a cooperative tilting of the corner shared octahedra such that structure distorts to orthorombic *Pnma* symmetry [4]. There are different ways in which the octahedra can tilt, each leading to a different coordination environment for the *A* site cation.

A standard notation of octahedral tilting has been developed to describe octahedral tilting by Glazer (1972) [5]. According to Glazer *S. G. Pnma* belongs to $a^-b^+a^-$ octahedra tilt system. This symbol indicates that rotations about axes *a* and *c* are for the same angle and rotation magnitude about axis *b* differs. A positive superscript would denote the neighboring octahedra tilt in the same direction (in phase) and a negative superscript implies the neighboring octahedra tilt in the oposite direction (out of phase).

In order to estimate the theoretical stability of the perovskite structure, Goldschmidt tolerance factors, G_t and global instability indices, *GII* were calculated for $Ca_{1-x}Y_xMnO_3$ solid solution, using the software SPuDS (Structure Prediction Diagnostic Software). In an ideal cubic perovskite, the ionic radii, r_i ($i = A, B, O$), satisfy the relation: $r_A + r_O = \sqrt{2}(r_B + r_O)$. The Goldschmidt tolerance factor for perovskites is, hence, defined by:

$$G_t = \frac{r_A + r_O}{\sqrt{2}(r_B + r_O)} \qquad (1)$$

When the radii of the A and B site cations fulfil the requirements of the Goldschmidt tolerance factor, $G_t = 1$, the perovskite will be stable and have a cubic symmetry [6]. According to [7] the perovskite structure may form in oxides for which $0.89 < G_t < 1.02$. Cation enters into position that results in G_t closer to 1.

It is expected from the tolerance factors that small rare earth (RE) ions with $r(RE^{3+}) \leq 0.87$ Å will occupy the *B* site, and large RE with $r(RE^{3+}) \geq 0.94$ Å will occupy the *A* site, while intermediate RE with $0.87 \leq r(RE^{3+}) \leq 0.94$ Å will occupy both sites with different partitioning for each ion (Fig. 1).
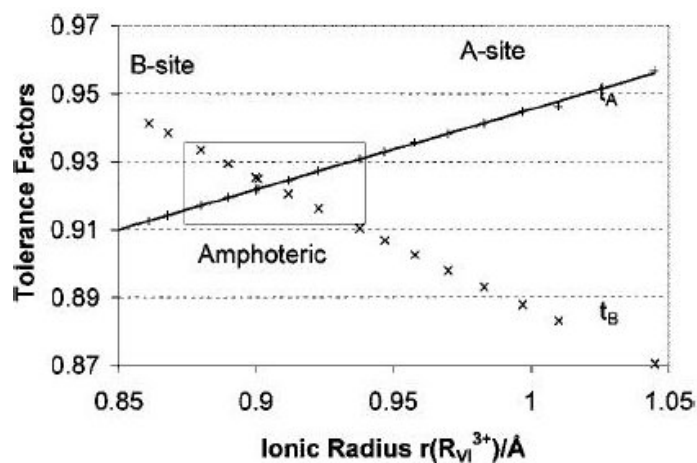
Fig. 1. The tolerance factors t_A and t_B for substitution of trivalent ions on the A and B sites as a function of the ionic radius [8].

The overall structure stability is determined by comparing the calculated bond-valence sums with the ideal formal valences [3]. This parameter is refered to as the global instability index (*GII*) and is calculated according to:

$$GII = \left\{ \left[\sum_{i=1}^{N} \left(d_i^2 \right) \right] \Big/ N \right\}^{1/2} \tag{2}$$

The variables involved in (2) are (d_i) the deviation from the valence sum rule, and N, which is the number of the atoms in the asymmetric unit. In the bond valence model the empirical correlation of equation (3) is used to determine the bond valence, s_{ij}, of a chemical bond from its lenght, R_{ij}:

$$s_{ij} = \exp\left(\frac{R_0 - R_{ij}}{B} \right) \tag{3}$$

where $B = 0.37$ and R_0 is the lenght of a bond of unit valence. The values of R_0 for most of the common bonds are tabulated in reference [9] and values of R_0 used in the present work for calculating the valence of the bond between Mn and O are listed in tab. I.

Magnetic characterization was performed using electron paramagnetic resonance (EPR). Because of nonmagnetic character of Y, EPR is an appropriate tehnique for this study.

Tab. I. The ionic radii and R_0 values used in this work for the bond between a cation and oxygen and the deviation, d_i, from the valence sum rule (equation 2) of the ion in the ideal perovskite structure.

	A(XII)		B(VI)		X(VI)
Ions	Ca^{2+}	Y^{3+}	Mn^{4+}	Mn^{3+}	O^{2-}
Ionic radii[Å] [12]	1.34	1.19	0.53	0.645	1.40
R_0	1.967	2.019	1.753	1.760	
d_i [13]	0.733	1.542	0	0	

Experimental procedure

We calculated Gt and GII using the software SPuDS and analysed the possibility of existence of perovskite structure type for projected nominal compositions. Samples were synthesized using modified glycine-nitrate procedure (MGNP) [10]. This method was used for synthesis of undoped (CM) and 10 (CY1M), 20 (CY2M) and 30 (CY3M) % Y doped nanopowders of CaMnO$_3$. We used nitrates of Ca and Y in the form of solutions, and Mn acetate and glycine in the form as received. The reactants were heated on a hot plate up to 540 ºC, until the evolution of the smoke terminated. The obtained ashes were afterwards calcined at 800 ºC for 2 hours. Phase analysis of the synthesized powders was done by X-ray powder diffraction (XRPD) on a SiemensD500 diffractometer with a Ni filter using Cu$_{K\alpha}$ radiation and the step-scan mode (2θ range: 4 - 90º). To derive the relevant structural

parameters, the experimental data for Rietveld refinement were taken afterwards in the angular range 20 – 90 °2θ, with a step width of 0.025 °2θ and 5 s per step. Structural analysis was carried out using Rietveld refinement and the program FullProf [11]. EPR measurements were performed on the CM calcined at 1100 °C, CY2M and CY3M samples using a Varian E-line spectrometer operating at a nominal frequency of 9.5 GHz. TEM was carried out by using a JEOL JEM 2010 200 kV microscope.

Results and discussion

Using SpuDS we calculated G_t and global instability index *GII*, for all members of the investigated solid solution. For cations in position *A* of the perovskite structure (Ca^{2+} and Y^{3+}) the program considers ionic radii for *C. N.* 12, and for cations in position *B* of investigated structure type (Mn^{4+} and Mn^{3+}) octahedral enviroment. All these values, together with R_0 i d_i that are neccesary for calculating *GII* , are given in table I.

SPuDS can calculate G_t and *GII* for 0, 25, 33, 50, 67, 75 i 100 mass. % Y. Graphical representation of G_t and *GII* as a function of Y content is given in Fig. 2. The calculated values for our nominal compositions were obtained using interpolation procedure (table II). Obtained values for G_t and *GII* satisfy conditions for existence of perovskite structure type for all synthesized oxides. Since the calculated G_t is smaller than 1 it will result in deformation of ideal cubic cell. G_t for CaMnO$_3$ is closest to 1 and has the lowest *GII* indicating that this perovskite structure is less distorted and distortion increases with entering Y in the structure. CaMnO$_3$ is orthorombic, *S. G. Pnma* [14, 15]. The small ionic radius of Y^{3+} results in a small value of the tolerance factor leading to instability of the perovskite structure. Calculated value of G_t for YMnO$_3$ is 0.88, and that is out of range for existence of perovskite structure type for oxides. At atmospheric pressure YMnO$_3$ crystallizes in hexagonal structure and upon annealing under high pressures can be converted to its orthorombic phase [16]. Both structures are nonperovskite. Y doped CaMnO$_3$ is orthorombic [17, 18, 19], and as a result of Y doping G_t decreases up to the limit value for the existence of perovskite structure type. The structure can tolerate Y in CaMnO$_3$ until 0.75 mass. % in the position *A*. Higher concentrations of Y provoke segregation of YMnO$_3$. *GII* increases with the Y content increase. This indicates an increase of the structure instability as a consequence of the presence of cations with different size and valence.
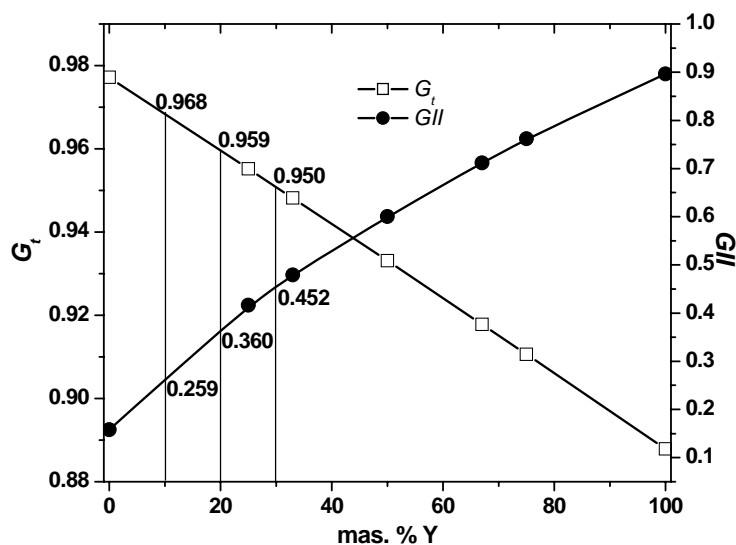
Fig. 2. Y content versus G_t and *GII*.

Tab. II. Calculated values of G_t and *GII* for synthesized (*) perovskite phases and end members.

Composition	G	*GII*
$CaMnO_3{}^*$	0.97	0.15
$Ca_{0.9}Y_{0.1}MnO^*$	0.96	0.25
$Ca_{0.8}Y_{0.2}MnO^*$	0.95	0.36
$Ca_{0.7}Y_{0.3}MnO^*$	0.95	0.45
$YMnO_3$	0.88	0.89

Rietveld refinement revealed that all perovskite phases are orthorombic with space group *Pnma*. The best fits between calculated and observed X–ray diffraction patterns for investigated samples are given in Fig 3. All allowed Bragg reflections are shown by vertical bars. By inspecting difference between the experimental and calculated profiles, good agreement can be observed. Correctness of the fit can be monitored by the reliability (*R*) factors that are given as inset and also indicate high reliability of the refinement results.
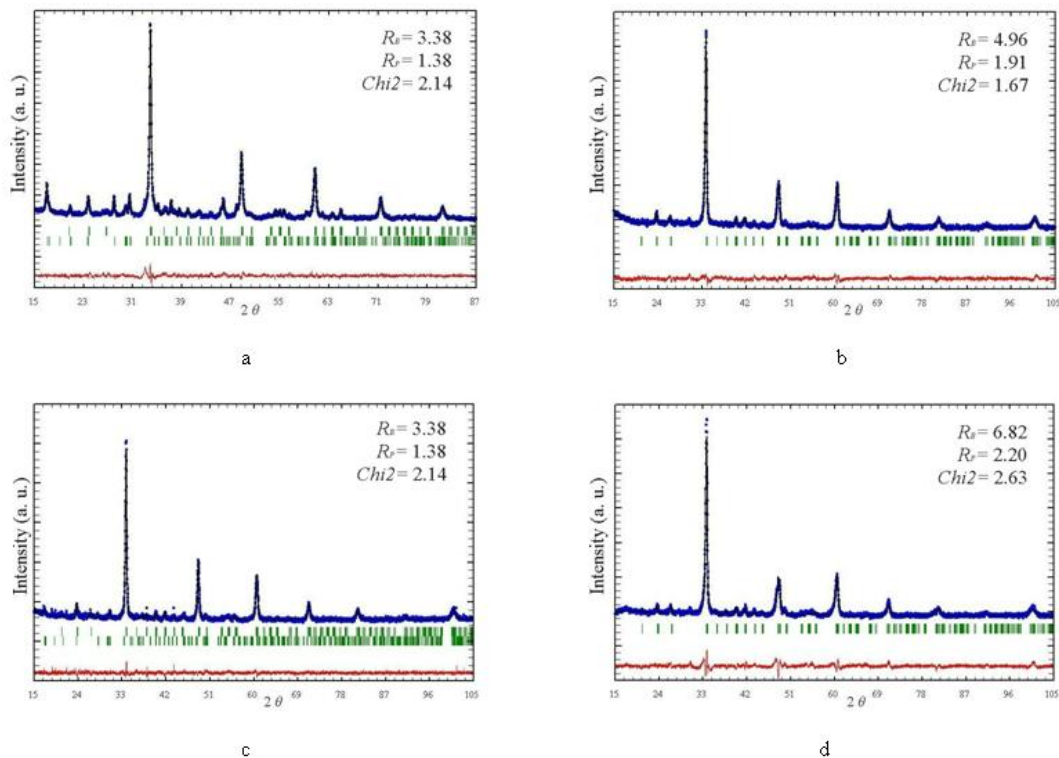
Fig. 3. Rietveld diagram for a) CM; b) CY1M; c) CY2M and d) CY3M sample.

Quantitative phase analysis revealed that besides perovskite phase CM sample contains 26.9(3) mass % of $Ca_2Mn_3O_8$, CY1M contains 8,6(2) mass % of $Ca_2Mn_3O_8$ and CY2M and CY3M contain only perovskite phase (Fig. 3). Crystallographic data and results of Rietveld refinement for investigated samples are given in tab. III.

Tab. III. Unit cell parameters, unit cell volume and atomic positions for investigated samples.

	CM	CY1M	CY2M	CY3M
a	5.2819(6)	5.3067(3)	5.2955(7)	5.3213(9)
b	7.4600(5)	7.4725(7)	7.5217(5)	7.4675(6)
c	5.2778(6)	5.2813(4)	5.2804(6)	5.3075(8)
V	207.96(4)	209.42(3)	210.33(4)	210.91(5)
Ca				
x	0.027(1)	0.0308(8)	0.0332(8)	0.0392(9)
y	0.25	0.25	0.25	0.25
z	-0.026(1)	-0.017(1)	-0.011(2)	-0.015(2)
Mn				
x	0	0	0	0
y	0	0	0	0
z	0.5	0.5	0.5	0.5
O1				
x	0.497(3)	0.489(3)	0.420(3)	0.467(5)
y	0.25	0.25	0.25	0.25
z	0.023(4)	0.045(3)	0.122(3)	0.127(5)

The differences in unit cell parameters and consequently in unit cell volume are the result of the different amount of Y in each of these phases. Ionic radius of Y^{3+} is smaller than Ca^{2+} (table I). As a result of entering Y in the structure, a decrease of unit cell volume may be expected. But this is not the case, since doping with Y^{3+} provokes reduction of equivalent amount of Mn^{4+} to Mn^{3+} with larger ionic radius. So, the increase in unit cell volume is a consequence of reduction of Mn^{4+} to Mn^{3+}.

The large cations, Ca and Y occupy the $4c$ (x, ¼, z) position and the oxygen atoms are in two non-equivalent positions: O(1) at $4c$ (x, ¼, z) and O(2) at $8d$ (x, y, z). Refined coordinates are given in table III.

As results of Rietveld refinement interatomic distances and angles are obtained. Mn–O distances and angles were followed in order to analyse influence of Y on octahedra tilting magnitude. Tab. IV contains characteristic distances and angles between Mn, O1 and O2

atoms. Average values of interatomic distances Mn–O change with Y amount in the structure, and has the highest value in CY3M sample, where the content of Y is largest.

Tab. IV. Interatomic distances and bond angles for investigated samples ([*]Values in brackets are a measure of the degree of anisotropy).

Perovskite		CM	CY1M	CY2M	CY3M
<Mn–O>		1.921	1.919	1.915	1.934
Mn–O	2×	1.801(1)	1.788(1)	1.711(2)	1.674(1)
	2×	2.093(1)	2.084(1)	2.086(2)	2.141(1)
	2×	1.869(2)	1.884(2)	1.949(1)	1.992(1)
O2–Mn–O2		87.47	88.50	88.69	88.11
Mn–O1–Mn		172.41	165.11	149.44	139.21
Mn–O2–Mn		146.96	150.35	159.89	160.04
Mn (BVC)			4.04	4.23	4.23
Microcrystalline size [Å]		237.5(2)[*]	477.4(9)[*]	336.3(3)[*]	289.2(3)[*]
Microstrain ($\times 10^{-3}$)		1.612	2.519	2.387	2.744

Octahedra nets for all investigated samples are given in Fig. 4. Changes in angle values represent structural changes as a result of octahedral tilting. In ideal cubic structure Mn–O1–Mn and Mn–O2–Mn angles are 180º. As a result of octahedra tilting around all three axes in *S. G. Pnma*, these values are different. Mn–O1–Mn angle represents tilting around axis *b* and for investigated samples is the nearest to this value for $CaMnO_3$ in CM sample (table IV). With the increase of Y amount in the structure it differs more and more from 180º as a consequence of increased octahedra tilting magnitude. Magnitude of the octahedra tilting has the largest value in the CY3M sample, where the Y content is largest. Mn–O2–Mn angle represents octahedra tilting around axes *a* and *c*. Angle (magnitude of octahedra tilting) is the same around each of them, according to $a^-b^+a^-$ tilt system.
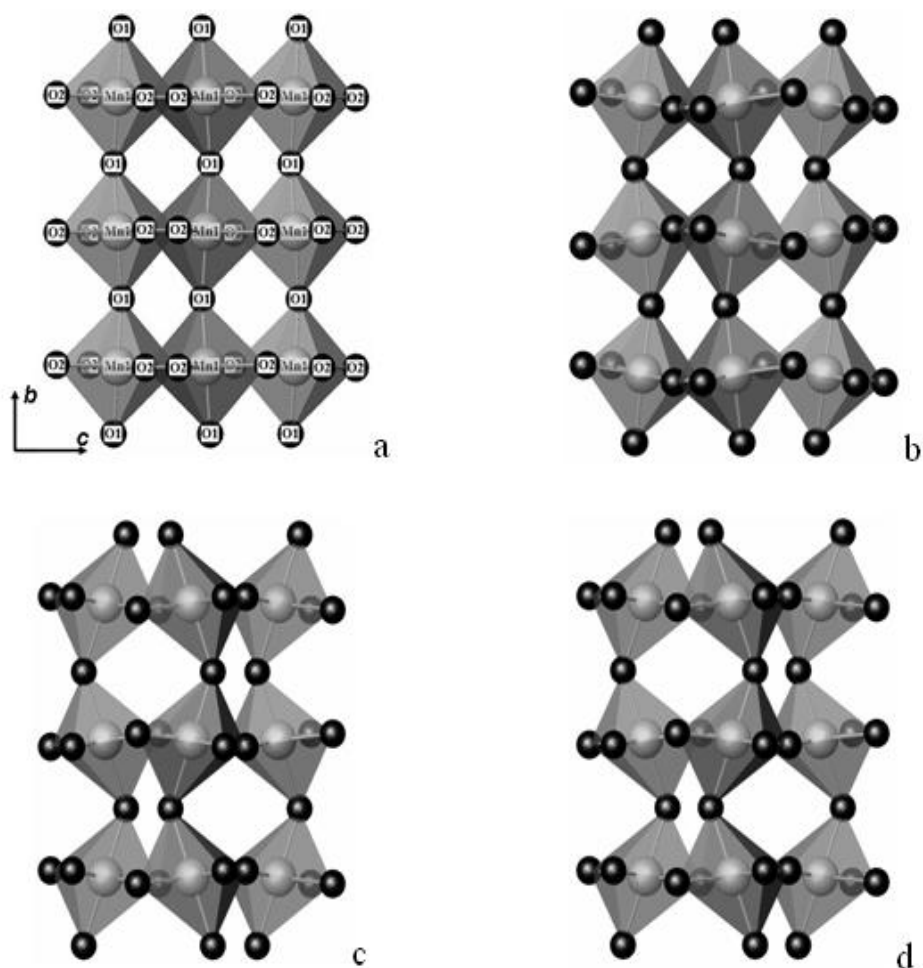
Fig. 4. Octahedra net for perovskite phase in a) CM; b) CY1M; c) CY2M and d) CY3M sample.

The influence of dopant concentration on octahedra deformations was analyzed. Interatomic distances Mn–O inside octahedra for all the investigated samples are shown in Fig. 5. First two bars are for interatomic Mn–O2 distance in the *ac* plane and here lies the longest and the shortest bond. The third bar represents Mn–O1 bond distance, in *b* axes direction, where the intermediate bond lies. Mn–O distances are direction dependent what results in octahedral deformation. The distortion of the octahedra is defined in the way that the deviation of the Mn–O (d_n) distances with respect to the average <Mn–O> ($<d_n>$) value is quantified [20]:

$$\Delta = (1/6)\sum_{n=1,6}\left[(d_n - \langle d\rangle)/\langle d\rangle^2\right]$$

(4)

The values of Δ are given in Fig. 5 above each bar. The difference between the longest and the shortest distance increases with the increase of Y and Mn^{3+} content in the structure. $CaMnO_3$ also shows octahedral deformation phenomenon, and this indicates that there is some amount of the Mn^{3+} in the structure and some amount of oxygen vacancies as well. This indicates that it should be better to observe $CaMnO_3$ as nonstoichiometric phase $CaMnO_{3-\delta}$ [21]. According to [20] the distortion of the octahedral parameter appears in the $Ca_{1-x}Y_xMnO_3$ system only for Y > 0.5. Octahedra deformation indicates the presence of this phenomenon

for smaller concentrations of Y, and reason for this may lie in the existence of oxygen vacancies that also may provoke reduction of Mn^{4+} to Mn^{3+}.
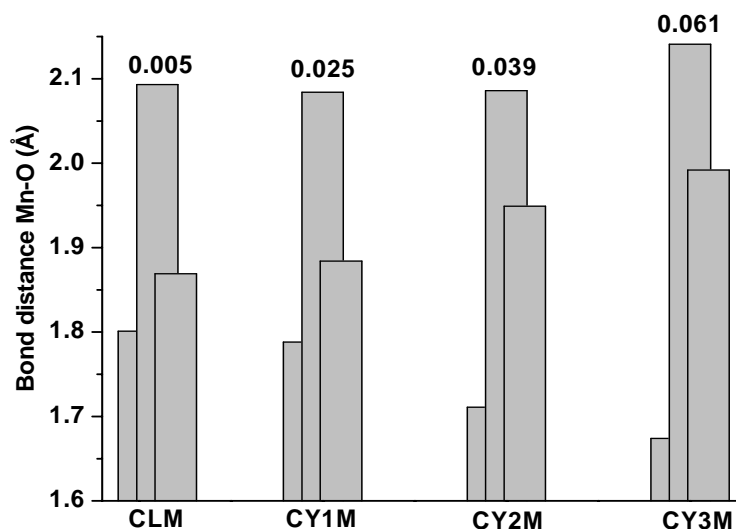
Fig. 5. Interatomic distance Mn–O for investigated samples.

Bond valence calculations resulted in Mn valence state that is higher than expected (Tab. IV). The presence of Mn^{3+} in CY1M, CY2M, CY3M perovskite phase should decrease the valence state of Mn. The valence state of Mn obtained from BVC calculations is often higher than nominal value and reason for this is strong Mn–O bond [22].

The EPR spectrum for all the samples consists of a single line with a g-factor close to 2 (Tab. V). Fig. 6 shows the EPR line at room temperature for different concentrations of Y, for the CM, CY2M and CY3M samples. The CM sample is fired at 1100 ºC in order to provoke phase transition of $Ca_2Mn_3O_8$ into $CaMnO_3$. Measured peak-to-peak line width is given also in Table V.

Tab. V. EPR line width and *g* factors.

Sample	CM	CY2M	CY3M
Line width (*G*)	1460 ± 100	1980 ± 100	2130 ± 100
g factor	1.982	1.997	2.000
Mn ions	Mn^{4+} $(3d^3)$	Mn^{4+} $(3d^3)$ $Mn^{3+}(3d^4)$	Mn^{4+} $(3d^3)$ $Mn^{3+}(3d^4)$

A continuous increase of the line width with increasing Y content is found. It seems that the origin of the EPR line widening can be searched in the crystal structure deformation. The increase of Y content in the samples leads to the increase of Mn^{3+} ion concentration and to the progressive octahedra distortion in the crystal lattice.
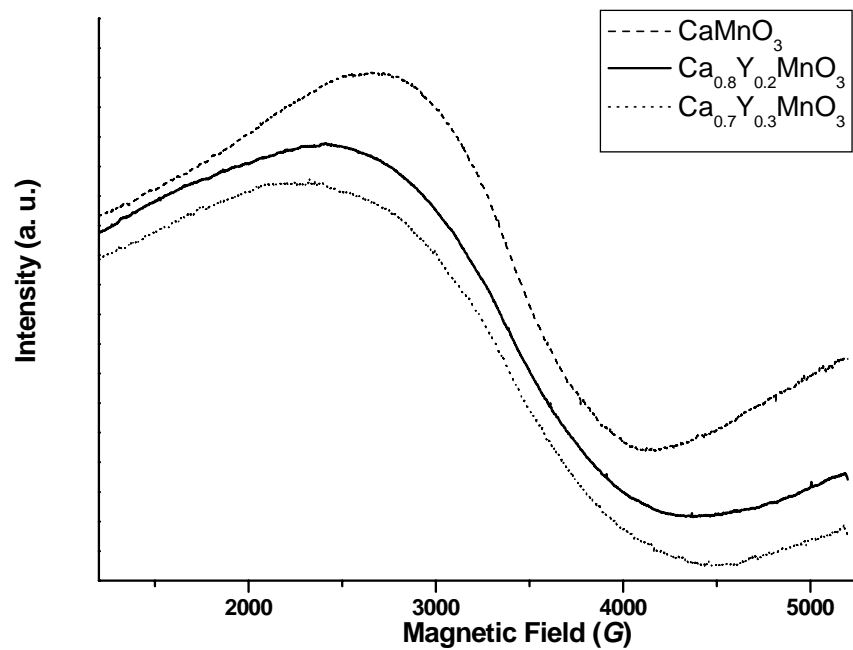
Fig. 6. EPR spectra for investigated samples.

XRPD line-broadening analysis was performed using the Rietveld method in conjunction with Warren-Averbach procedure in order to get crystallite size and lattice micro strain parameters. In the present approach the grain size broadening was represented by a Lorentzian function, and micro strain broadening by a Gaussian function. Obtained crystallite sizes are in nanometric range with crystallites of about 200-500 Å and microstrain increases with increasing Y amount (Table IV). TEM images of CY1M and CY2M samples in Fig. 7 confirm these results.

a   b
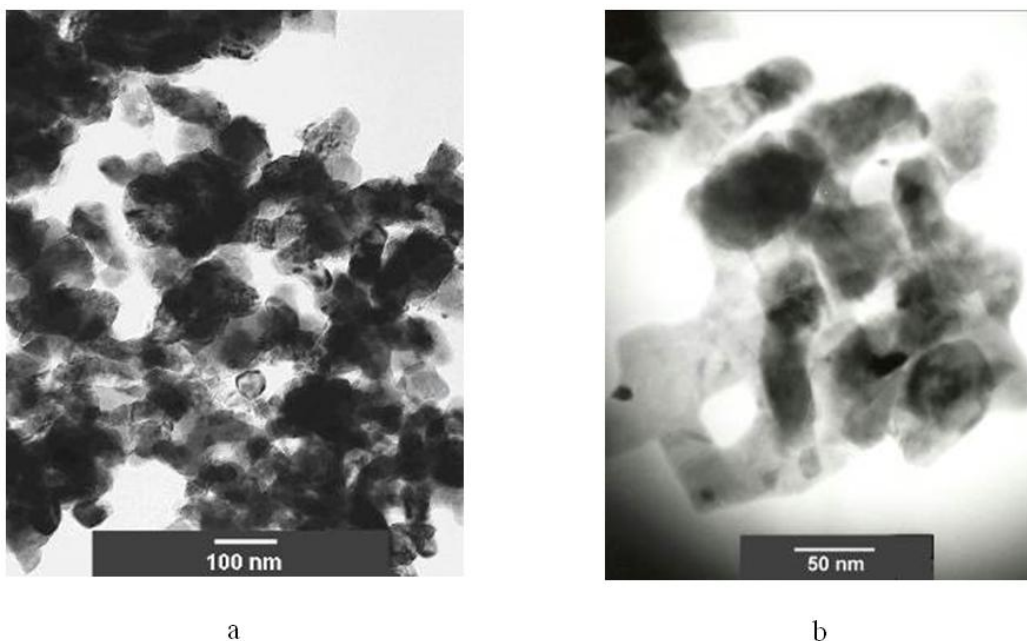
Fig. 7. TEM image of CY1M (a) and CY2M (b) sample.

Conclusions

The software SpuDS has been developed for predicting the structures of perovskite compounds and predicted structures can serve as the starting point for Rietveld refinements in the course of structural characterization of new materials. Calculating of G_t and *GII* can help in studying possibility of forming perovskite structure type. It also indicates the distortion from ideal cubic structure.

Influence of Y concentration on $Ca_{1-x}Y_xMnO_3$ (x = 0, 0.1, 0.2, 0.3) was analysed. The increase of unit cell volume with the increase of Y amount in the structure, ionic radius of which is smaller than Ca, is an evidence for the presence of Mn^{3+} in the structure. The difference in Mn electronic state overcomes the difference between ionic radii of Y and Ca. Higher content of Y^{3+} and Mn^{3+} in the structure increases octahedra tilting magnitude and structure deformation. Deformation of octahedra in $Ca_{1-x}Y_xMnO_3$ (x = 0, 0.1, 0.2, 0.3) points out to the presence of some Mn^{3+} in its structure.

The EPR line width broadening with increasing Y content can be understood in terms of the progressive distortion of the crystalline structure. The EPR line width seems to be a physical parameter that closely follows the cell distortion in $Ca_{1-x}Y_xMnO_3$.

The obtained CY1M and CY2M powders are in nanometric range, which is confirmed by the microstructural as well as by TEM analysis.

Acknowledgments

References

1. S. J. Hibble, S. P. Cooper, A. C. Hannon, I. D. Fawcett, M. Greenblatt, J. Phys.: Condens, Matter 11, (1999) 9221.
2. B. Raveau, A. Maignan, C. Martin, M. Hervieu, Chem. Mater. Vol.10 (1998) 2461.
3. M. W. Lufaso, P. M. Woodward, Acta Cryst. B 57 (2001) 725.
4. P. M. Woodward, Acta Cryst. B 53 (1997) 32.
5. A. M. Glazer, Acta Cryst. B 28 (1972) 3384.
6. M. Mogensen, D. Lybye, N. Bonanos, P. V. Hendriksen, F. W. Poulsen, Solid State Ionics 174 (2004) 279.
7. J. M. D. Coey, M. Viret, S. Von Molnar, Adv. Phys. Vol. 48, No. 2 (1999) 167.
8. Y. Tsur, T. D. Dunbar, C. A. Randall, J. Electroceram. 7 (2001) 25.
9. I. D. Brown, D. Altermatt, Acta Cryst. B 41 (1985) 244.
10. S. B. Bošković , B. Z. Matović, M. D. Vlajić, V. D. Krstić, Ceram. Int. Vol. 33 (1) (2007) 89.
11. J. Rodriguez-Carvajal: Collected Abstract of Powder Diffraction Meeting, Toulouse (1990) 127.
12. R. D. Shannon, Acta Cryst. A 32 (1976) 751.
13. G. H. Rao, K. Barner, I. D. Drown, J. Phys.: Condens. Matter. 10 (1998) L757.
14. H. Taguchi, M. Sonoda, M. Nagao, J. Solid State Chem. 137 (1998), 82-86.
15. J. Blasco, C. Ritter, J. Garcia, M. J. De Teresa, J. Perez-Cacho, R. M. Ibarra, Phys. Rev. Serie 3. B-Condens. Matter 62 (9) (2000) 5609.
16. M. N. Iliev, M. V. Abrashev, H. G. Lee, V. N. Popov, Y. Y. Sun, C. Thomsen, L. R. Meng, W. C. Chu, Phys. Rev. Serie 3. B-Condens. Matter 57 (1998) 2872.

17. M. Dlouha, S. Vratislav, Z. Jirak, J. Hejtmanek, K. Knizek, D. Sedmidubsky, Appl. Phys. A 74 (2002) S673.
18. P. M. Woodward, T. Vogt, D. E. Cox, A. Arulraj, C. N. R. Rao, P. Karen, A. K. Cheetham, Chem. Materi. 10 (1998) 3652.
19. S. J. Hibble, S. P. Cooper, A. C. Hannon, I. D. Fawcett, M. Greenblatt, J. Phys.: Condens. Mat. 11 (1999) 9221.
20. G. A. Maris: Structural Transition Induced by Charge and Orbital Ordering in Transition Metal Oxides. Ph. D. Thesis, (2004), University of Groningen, Netherlands.
21. M. E. Melo Jorge, A. Correia dos Santos, M. R. Nunes, Int. J. Inorg. Mater. 3 (2001) 915.
22. C. O. Paiva-Santos, R. F. C. Marques, M. Jr. Jafelicci, L. C. Varanda, Powder Diffr. 17 (2) (2002) 149.

Садржај: *Испитивана је структура и магнетне особине наноструктурних материјала са општом формулом $Ca_{1-x}Y_xMnO_3$ (x=0; 0,1; 0,2; 0,3). Коришћењем компјутерског програма SPuDS (софтвер за предвиђање структуре) израчунати су Голдшмитов фактор фактор толеранције, G_t и глобални индекс нестабилности, GII. На основу ова два параметра анализирана је могућност формирања перовскитског типа структуре за чврсти раствор $Ca_{1-x}Y_xMnO_3$. Улазак Y^{3+} на место Ca^{2+} доводи до редукције једнаке количине Mn^{4+} у Mn^{3+}, чије присуство је разлог за појаву многих интересантних магнетних, транспортних и структурних особина код допираног $CaMnO_3$. Структура је утачњена коришћењем Ритвелдове анализе. $Ca_{1-x}Y_xMnO_3$ (x=0; 0,1; 0,2; 0,3) кристалише у просторној групи Pnma, која према Глејзеровој класификацији спада у $a^-b^+a^-$ систем нагињања октаедара. Анализиран је утицај садржаја Y на углове и дужине веза Mn–O, нагињање MnO_6 октаедара око све три осе као и на деформацију октаедара. Да би се израчунало валентно стање Mn израчунате су валенце везе. Коришћењем ЕПР методе (електронске парамагнетне резонанце) урађена су магнетна мерења и анализиране магнетне особине чврстих раствора, степен орторомбичности јединичне ћелије, као и однос Mn^{4+}/Mn^{3+} катјона у положају Б у структури перовскита.Микроструктурна анализа је као резултат дала нанометарске димензије величине кристалита и микронапрезања што је и потврђено TEM микрофотографијама.*
Кључне речи: *Наноструктурни материјали, Ритвелдова анализа, Рачунање валенце веза, Магнетне особине.*